COMPUTER METHODS AND PROGRAMS IN BIOMEDICINE 99 (2010) 219–229

journal homepage: www.intl.elsevierhealth.com/journals/cmpb

Studying the properties of the updating coefficients in the OSEM algorithm for iterative image reconstruction in PET

Anastasios Gaitanis[e,b], *George Kontaxakis*[c,d], *George Spyrou*[b], *George Panayiotakis*[e], *George Tzanakos*[a,*]

[a] *University of Athens, Department of Physics, Division of Nuclear & Particle Physics, Panepistimioupoli, Zografou, Athens 15771, Greece*
[b] *Biomedical Research Foundation of the Academy of Athens (BRFAA), Soranou Efessiou 4, Athens 11527, Greece*
[c] *Universidad Politécnica de Madrid, E.T.S.I. Telecomunicación, Dpto. Ingeniería Electrónica, 28040 Madrid, Spain*
[d] *Networking Research Center on Bioengineering, Biomaterials and Nanomedicine (CIBER-BBN), Madrid, Spain*
[e] *Department of Medical Physics, Medical School, University of Patras, 265 00 Patras, Greece*

ARTICLE INFO

Article history:
Received 27 April 2009
Received in revised form
4 October 2009
Accepted 13 November 2009

Keywords:
Positron emission tomography
Image reconstruction
Monte Carlo
Ordered subsets expectation maximization
Pixel updating coefficients

ABSTRACT

We have studied the properties of the pixel updating coefficients in the 2D ordered subsets expectation maximization (OSEM) algorithm for iterative image reconstruction in positron emission tomography, in order to address the problem of image quality degradation—a known property of the technique after a number of iterations. The behavior of the updating coefficients has been extensively analyzed on synthetic coincidence data, using the necessary software tools. The experiments showed that the statistical properties of these coefficients can be correlated with the quality of the reconstructed images as a function of the activity distribution in the source and the number of subsets used. Considering the fact that these properties can be quantified during the reconstruction process of data from real scans where the activity distribution in the source is unknown the results of this study might be useful for the development of a stopping criterion for the OSEM algorithm.

1. Introduction

Positron emission tomography (PET) produces quantitative images that illustrate the distribution of a radiopharmaceutical in a living organism that are employed for the extraction of physiological or pathological information. PET imaging is used in a wide area of medical disciplines such as oncology, neurology, cardiology, and drug development [1–4].

PET images are produced following data acquisition in a process known as image reconstruction. In contrast with earlier systems where analytical algorithms have been employed (such as filtered back projection (FBP), and directly adapted from X-ray computerized tomography systems), modern PET systems typically employ iterative image reconstruction algorithms based on statistical algorithms that better suit the Poisson nature of positron emissions. A drawback of these algorithms as compared to conventional analytical solutions has been their high computational complexity. Due, however, to the constant improvement of computing technologies, efficient programming methodologies and clever implementation techniques that employ symmetries [5] and other modeling aspects, this weakness has been currently partially overcome.

Iterative image reconstruction algorithms initially calculate a first estimation of the radioactivity distribution in the source. This estimation is then forward-projected and there-

* *Corresponding author*. Tel.: +30 210 7276938.
E-mail address: tzanakos@phys.uoa.gr (G. Tzanakos).
0169-2607/$ – see front matter
doi:10.1016/j.cmpb.2009.11.011

upon the new estimated projections are calculated. In each iteration the estimated and measured projections are compared and a new estimate of the radioactivity distribution is calculated. This procedure is repeated until a pre-defined number of iterations have been performed or until the optimum image has been obtained according to a pre-defined criterion. The iterative algorithms that have been widely used in PET scanners are the maximum likelihood expectation maximization (MLEM) [6] and ordered subsets expectation maximization (OSEM) [7].

The main advantage of iterative algorithms is that they incorporate a model of the acquisition process in the image reconstruction task. In PET imaging, the data acquired have Poisson nature and the image quality is affected by attenuation, scatter and random coincidence effects. The entire acquisition process can be modeled in the system matrix α. Each element of this matrix represents the probability that a gamma ray emitted by a pixel i is detected by a specific pair of scintillation detectors in opposite positions, forming a line of response (LOR) j. The MLEM algorithm solves the problem of image reconstruction by producing an estimate of the true activity distribution in the source that would maximize the probability to observe the measured counts. The OSEM algorithm represents an accelerated variant of the MLEM algorithm, where the projection data are grouped into subsets. The incorporation of an accurate model of the acquisition procedure in the system matrix, allows the MLEM and OSEM algorithms to produce images with fewer artifacts than FBP. On the other hand, iterative algorithms demonstrate a noise degradation of the images produced as a result of the iterative process. Various methods have been investigated for solving this problem. One possible way is to stop the reconstruction after an arbitrary number of iterations and then post-filter the resulting image [8]. The most attractive method of this category is the replacement of the ML criterion with a maximum posteriori (MAP) criterion by applying a Bayesian prior [9,10]. A second method is to stop the reconstruction, based on a specific stopping rule.

The present work deals with the study of several properties of the updating coefficients in the OSEM algorithm that potentially can give insights in the development of a stopping rule for this iterative procedure. Different research groups have tried to develop several stopping rules for the MLEM algorithm, however to the best of our knowledge, there is no published work on the development of a stopping rule for the OSEM algorithm.

In 1987 and 1988 Veklerov and Llacer [11,12] proposed two stopping rules for the MLEM algorithm, both based on the minimization of two specific figures of merit (FOM). The first FOM was part of the Pearson's χ^2 test and the second was a parameter similar to root mean square (RMS) error. Holte et al. [13] proposed a stopping rule for the MLEM algorithm based on a parameter that takes into consideration the pixel values of both the initial and reconstructed images. According to this assumption this stopping rule cannot be employed in studies with real data, because the true activity distribution in the source is unknown. Moreover, Bissantz et al. [14] studied a stopping rule for the MLEM algorithm by taking into account the residuals between the forward projected image and the measured counts in each row of the sinograms. Finally, our research group has also published works [15–18] on a new stopping rule for the MLEM algorithm that focus on the pixel updating coefficients generated in the iterative process. In our last paper [18], the behavior of the updating coefficients was studied versus different image activities and the result was a quantitative relationship among them. Based on this assumption a stopping rule was developed. The proposed methodology has been found to work quite well independent of the level and the shape of the activity distribution in the source and the stopping rule was found to depend only on the total number of counts in each image. Motivated by this, the study of the properties of the pixel updating coefficients has been expanded for the case of the OSEM algorithm, which in fact represents an accelerated version of the MLEM algorithm. In practice, most clinical systems that employ iterative image reconstruction utilize the OSEM algorithm instead of the MLEM. Since the latter can be considered a special instance of the OSEM algorithm (with number of subsets equal to one), it is essential to study the behavior of the pixel updating coefficient when employing a variable number of subsets.

This paper is organized as follows: in the subsequent section there is a brief summary of the OSEM algorithm, the model of the PET scanner employed, the methodology for the calculation of the system matrix and the coincidence data generation using Monte Carlo techniques. Section 7 presents the results obtained from the analysis of the properties of the pixel updating coefficients and focuses on the behavior of their minimum value for the non-zero pixels in the phantom image. The discussion makes evidence that a correlation can be found between the minimum value of the updating coefficients vector and the quality of the reconstructed images.

2. Ordered subsets expectation maximization (OSEM)

In the OSEM algorithm the data are grouped into ordered subsets (OS). Consequently, the same procedure applied in the pixel updating scheme of the MLEM algorithm is then applied to the data of each of these subsets. The image acquired after the first sub-iteration over one subset, constitutes the initial image of the pixel updating scheme which employs the data of the next subset and so on. The image obtained after one iteration over n subsets in the OSEM algorithm, has been observed to be visually similar to the image resulted after n iterations of the MLEM algorithm over the complete set of data acquired in the PET scan.

Let $\mathbf{x}^0$ be a uniform initial image, and $\mathbf{x}^{(k)}$ be an estimation of the true activity distribution $\mathbf{x}$ after k iterations. In addition, let $S_1, S_2, \ldots, S_n$ represent the nth subset to which the data vector y has been divided into, $i = 1, 2, \ldots, I$ be the image pixels and $j = 1, 2, \ldots, J$ the lines of response. With the above definitions the mathematical formulation of the OSEM reads [7]:

$$x_i^{(k)} = x_i^{(k-1)} C_i^{(k-1)} \tag{1}$$

$$C_i^{(k-1)} = \frac{1}{\sum_{j \in S_n} a_{ij}} \sum_{j \in S_n} \frac{a_{ij} y_j}{\sum_{i'=1}^{I} x_{i'}^{(k-1)} a_{i'j}} \tag{2}$$

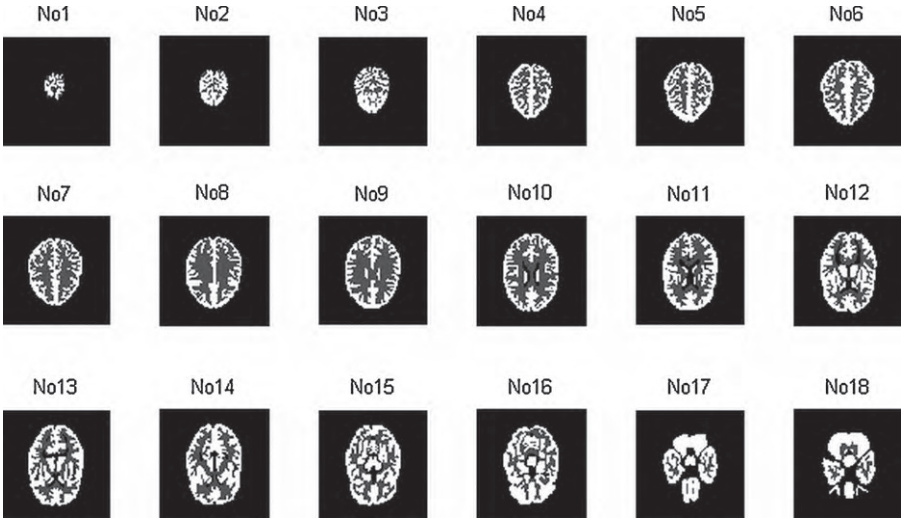

Fig. 1 – The eighteen slices of Hoffman brain phantom.

where y_j represents the projected data in jth line of response and α_{ij} is the system matrix element. The coefficient $C_i^{(k-1)}$ updates the value of the ith pixel at iteration k. Eq. (2) shows that $C_i^{(k-1)}$ depends only on the observed counts y_j in each subset and on the system matrix element α_{ij} that corresponds to that particular pixel and line of response, the value of which is calculated once, during the initialization time. In studying the behavior of the updating coefficients of the OSEM algorithm for different number of subsets, we expect to have a first indication about the correlation of the coefficient C and the number of subsets. This is a study that further expands the one that we performed about MLEM.

3. PET scanner configuration

For the study of the behavior of the pixel updating coefficients in the OSEM algorithm, a single-ring PET scanner was simulated. The detector ring was composed of 128 scintillator crystals with widths of 7.36 mm each. The size of the field of view (FOV) was 200 mm × 200 mm. The radius of the detector ring was 150 mm. The number of all possible lines of response (LORs) was 8128. The image array size was 128 × 128 pixels that each has a size of 1.56 mm. Monte Carlo methods was used to simulate the operation of the PET scanner: the activity distribution in the source, the generation of annihilation events, the gamma ray propagation and detection by the scintillator detectors. All noise sources (Compton scattering, photoelectric effects and random coincidences) have not been taken into consideration. Two-dimensional (2D) data acquisition has been assumed for this case, which corresponds to the case of PET acquisition with septa.

4. The system matrix α

The system matrix depends entirely on the configuration and the geometry of the PET scanner. For the calculation of the system matrix Monte Carlo methods were used. In every pixel of the image grid, 1×10^7 annihilation events were uniformly generated and the resulting gamma rays isotropically distributed in the 2D space. Each element of the system matrix represents the transition law from the image activity distribution to the detected counts. A given matrix element, α_{ij}, is estimated from:

$$a_{ij} = \frac{N_{ij}}{N_{tot}} \tag{3}$$

where N_{ij} is the number of gamma rays emitted by the ith pixel and detected by the jth LOR, while N_{tot} is the total number of gamma rays generated in the area of the ith pixel.

5. Generation of the projection data

For this study the digital Hoffman brain phantom was used [19]. This phantom is composed of eighteen slices as shown in Fig. 1. The pixel value in the phantom image corresponds to the activity distribution in the area covered by this pixel. Using Monte Carlo methods, pairs of gamma rays were generated in numbers proportional to the corresponding pixel values.

For the simulation of gamma ray propagation, a dedicated algorithm was developed. This algorithm generated the annihilation events of the phantom active areas (areas with non-zero activity distribution level). Once a pair of gamma rays was produced, its propagation to the detectors was simulated and the vector of the projection data was updated. The detector efficiency was assumed to be 100% and the OSEM algorithm was used to reconstruct the image from the generated projections.

6. Software implementation and hardware requirements

For the development of the algorithms that were essential for the simulation process the computer language ANSI C was used. For the analysis of the histograms of C values, the

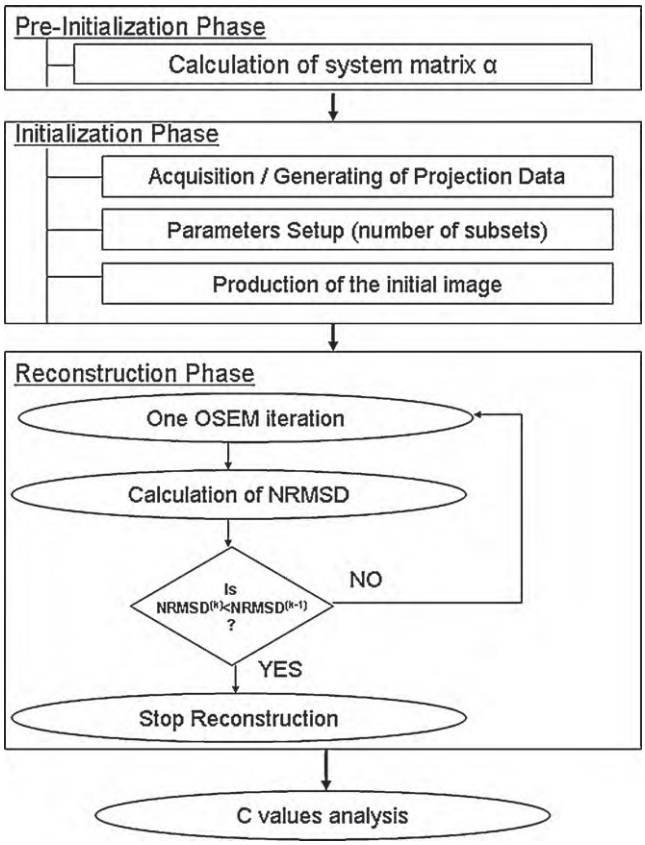

Fig. 2 – Logic flowchart of the proposed algorithm. The decision box was used to produce the results of Figs. 11 and 12. For all other figures the decision box is not valid.

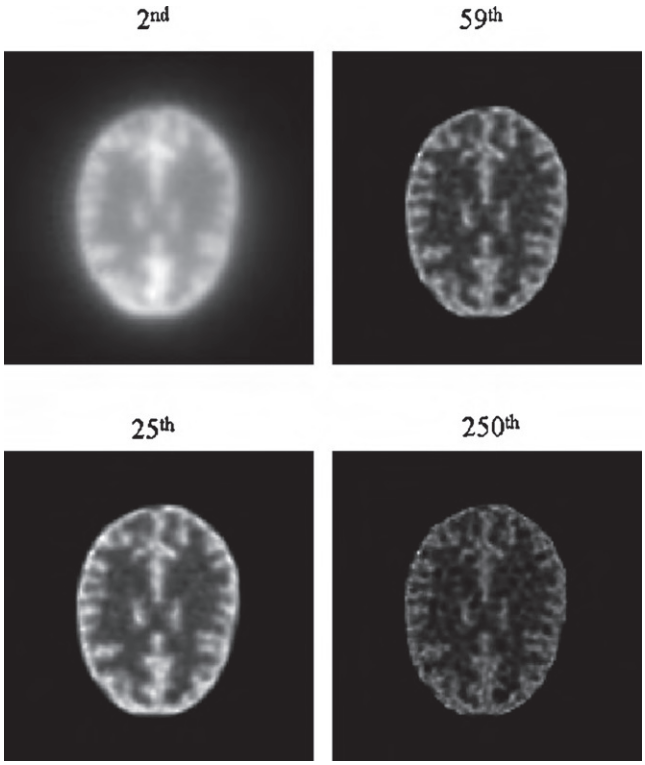

Fig. 3 – Hoffman brain phantom slice 9, with 1 M counts activity, reconstructed after 2, 25, 59 and 250 iterations.

free software ROOT v4.0/08 [20] was utilized. A PC platform has been employed, equipped with a Pentium 4 at 3.0 GHz, 1.5 GB RAM, under the Microsoft Windows XP (Version 2002) operating system. The memory requirement for the calculation of system matrix α for the image size of 128×128 pixels, was approximately 1.065 GB. The size of the produced system matrix was 1.11 GB. In order to optimize the memory requirements and the matrix size, a sparse matrix technique has been used, where the stored system matrix was coded in three different sub-matrices. One was for the pixel i, one for the line of response j – where the emitted gamma rays from pixel i were detected – and one matrix for the value corresponded to a specific pair i, j was stored. The total size of the three sub-matrices was 56.5 MB (16.1 + 14.9 + 25.5 MB). The logic flowchart of Fig. 2 presents the methodology that was used to produce the results of Figs. 11 and 12. For the results presented in all other figures, the decision box in the flowchart is not valid. Instead, the algorithm ran for a predetermined number of iterations.

7. Results

When employing the OSEM algorithm on the generated data, the image quality initially improves as the number of iterations increases. However, if the iterations continue after a certain point, the resulting images become noisier. This is demonstrated in Fig. 3 where the reconstructed images after 2, 25, 59 and 250 iterations are shown for slice 9 of the Hoffman phantom with 1 M counts and 2 subsets. The images after the initial iterations are quite smooth and at around the 60th iteration reach their best quality. After this point, the image quality deteriorates. This phenomenon can be quantitatively described by using the normalized root mean squared deviation (NRMSD). Other research groups have also used a similar figure of merit [21,22]. In their works, these groups used the averaged mean square error, which measures the difference between the reconstructed and phantom image in a scale. When the phantom image changed, the scale was also changed and the comparison of noise levels between two different reconstructed images was not straightforward. In this paper we further improve this figure of merit weighing with the sum of squared pixel values of the phantom image. In this way, the NRMSD measures the difference between the reconstructed and phantom image, normalized to values between 0.0 and 1.0, which allows the comparison of image differences between various reconstruction parameters (image activity and number of subsets):

$$\mathrm{NRMSD} = \sqrt{\frac{\sum_{i=1}^{I}(x_i - \hat{x}_i)^2}{\sum_{i=1}^{I}\hat{x}_i^2}} \tag{4}$$

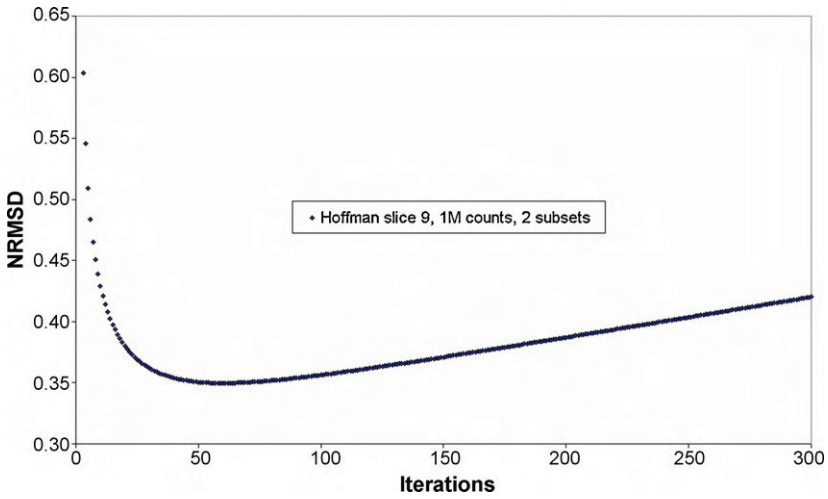

Fig. 4 – NRMSD versus number of iterations for Hoffman slice 9 with activity of 1 M counts.

where $\mathbf{x}$ and $\hat{\mathbf{x}}$ are the reconstructed and phantom image vectors respectively and i is the pixel number.

Theoretically, the best achievable image corresponds to the one obtained when NRMSD reaches its minimum. Fig. 4 shows that for the images obtained from data generated from the Hoffman slice 9 (using OSEM with 2 subsets) the NRMSD decreases up to the 59th iteration. After this point, the NRMSD increases, demonstrating a quantitative measure of the image deterioration due to the added noise. It is obvious that the NRMSD can be used only in studies in which the true activity distribution is known, therefore it cannot be used as a figure of merit for the monitoring of the image quality in real PET scans.

The phenomenon of the image deterioration led research groups to propose the stopping of the OSEM algorithm after a pre-defined number of iteration [23]. In this case, however, the reconstruction process does not take into consideration the special characteristics of each data set. Analyzing the behavior of the NRMSD for various data sets in the case of simulated data from the Hoffman brain phantom, we observed that the appropriate number of iterations depends on the total activity in the source and its distribution in the phantom image. Fig. 5a shows the NRMSD curves obtained for slices 2, 9, and 14 of the Hoffman brain phantom simulated for 1 M counts and employing two subsets for OSEM-based image reconstruction. Fig. 5b presents the data obtained from slice 9 at 1 M, 3.2 M and 6 M counts respectively. This shows that the best images are obtained at different iteration numbers, according to the minimum NRMSD criterion. It demonstrates that the convergence rate of the OSEM algorithm depends on the activity distribution in the source and on the total number of counts. The afore-mentioned observation led us to study here the behavior of the updating coefficients of the OSEM algorithm as a function of the source activity distribution levels.

The histograms in Fig. 6 show the distribution of the values of the updating coefficients C for reconstructed images from the Hoffman brain phantom slice 9 (6 M counts, 2 subsets) at iterations 5, 10, 20 and 40. Similarly, Fig. 7 shows the corresponding histograms when selecting 8 subsets for the same datasets. These values of C correspond to the non-zero pixels of the reconstructed image. From these histograms one can observe that there are two well identified regions: (i) one around $C_i \approx 1.0$ that corresponds to the image pixels for which reconstruction has produced a good approximation with their true value in the phantom distribution, and (ii) a tail with values $C_i < 1.0$ that corresponds to pixels for which such convergence has not yet been achieved.

In order to study the effect of Poisson noise on the reconstructed images, we have used the Hoffman slice 10 for simulations at two different activity distribution levels with a total of 100k and 200k counts respectively, and we created five different realizations for each case, adding randomly Poisson

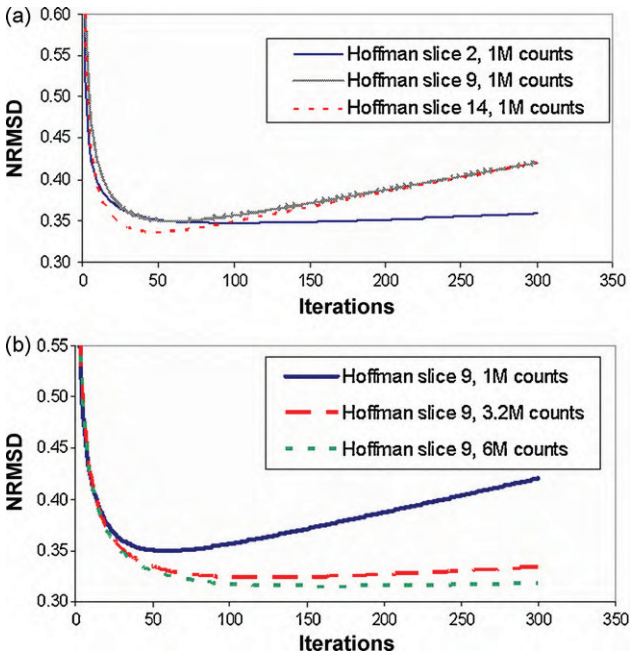

Fig. 5 – NRMSD versus number of iterations for: (a) three Hoffman brain phantom slices with the same activity and (b) Hoffman brain phantom slice 9 with different activities.

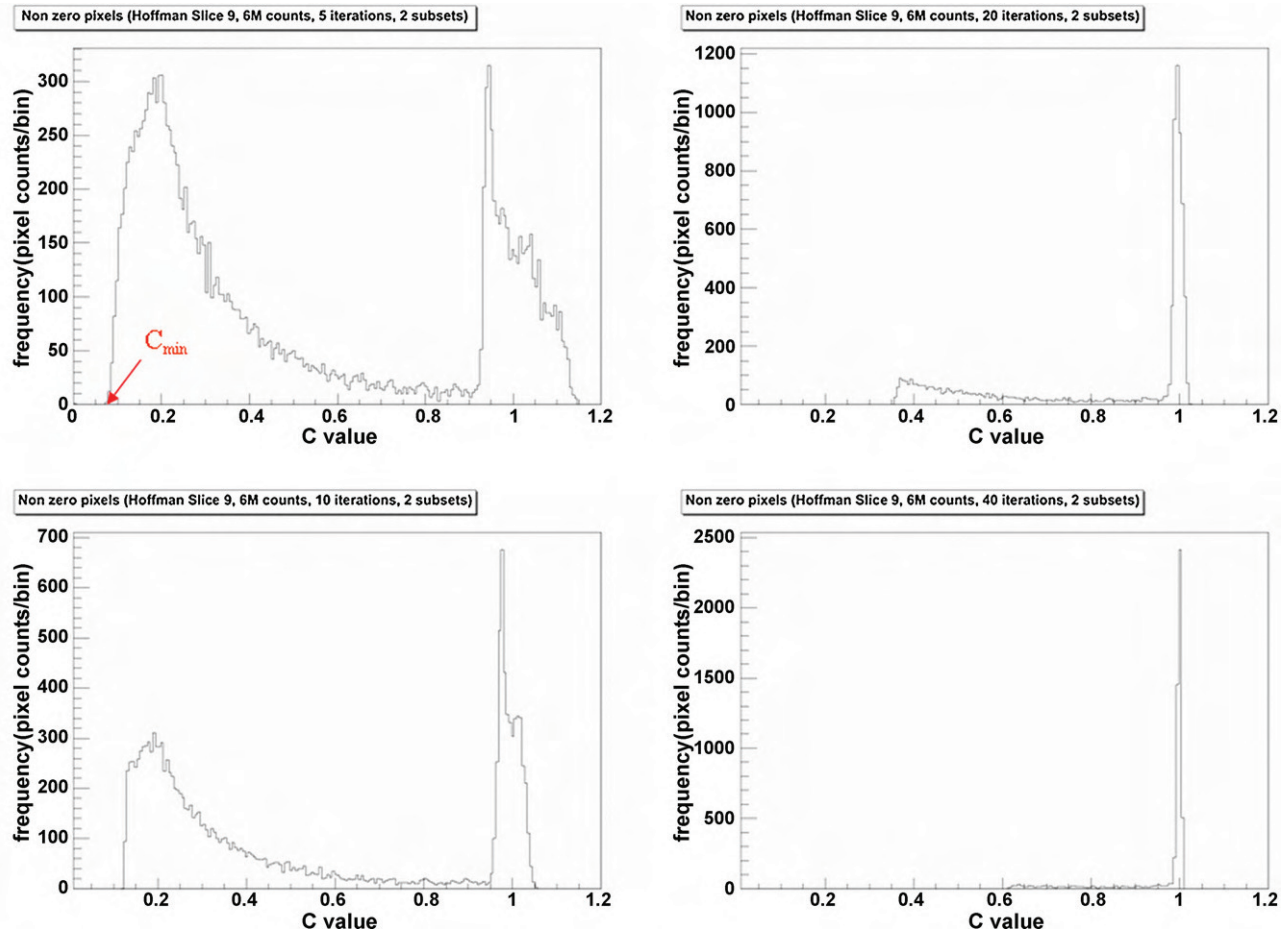

Fig. 6 – Histograms of the updating coefficients, C, at different iteration numbers for Hoffman slice 9 reconstructed with OSEM and 2 subsets. The leftmost non-zero bin in each histogram is defined as C_{min}.

noise in the data. In this way, we had six (one noise-free and five with Poisson noise) realizations for each activity distribution level. The Poisson noise was added as follow: in each non-zero pixel of noise free image, a new randomly value was created based on Poisson distribution. For each non-zero pixel, the Poisson distribution had as mean value the pixel value and as standard deviation the square root of the mean value. Then, we reconstructed all images for 250 iterations with 2 subsets and we then plotted the graphs of C_{min} versus iterations and the NRMSD versus iterations. As shown in Fig. 8, for the case of 100*k* counts (Fig. 8a), the minimum NRMSD is reached after 20 iterations, while for the case of 200*k* counts (Fig. 8b), this occurs after 25 iterations. It is clear that there is a small dependence of NRMSD versus iterations especially at small number of counts, as expected from Poisson statistics. This effect becomes smaller as the number of counts increases. Similar observations can be made regarding the behavior of C_{min} against iterations. As demonstrated in Fig. 8, the C_{min} values for the case of Poisson noise and noise-free data are similar at the iteration at which the NRMSD reaches at its minimum value. As the total number of counts in the data is increased, the variations between C_{min} and NRMSD curves are negligible. Our study is based on the record of C_{min} values against the minimum NRMSD. The plots of Fig. 8 show that Poisson noise causes no significant modifications on the behavior of the updating coefficients *C* on the iteration of interest and hence the effect of Poisson noise in the data can be considered negligible.

In Fig. 9, the minimum value, C_{min}, of the updating coefficients vector for each iteration, is plotted as a function of the NRMSD. We used the Hoffman slice 14 with 6 M counts activity and the image was reconstructed with 2, 4, 8 and 16 subsets. In these graphs, we observe three important features:

(1) The NRMSD is decreasing, with C_{min} monotonically increasing. There comes one iteration where the NRMSD is minimum and that value corresponds to a unique value of $C_{\min}^{opt}$, which is defined below. It is clear that the number of iterations where the minimum NRMSD is obtained varies with different number of subsets (see red arrows).
(2) This behavior is similar for different activity levels, and the minimum NRMSD is reached with fewer iterations for 16 subsets than for 2 subsets.
(3) As the number of subsets is decreased, the NRMSD gets lower values meaning lower noise level in the images, consistent with Poisson statistics.

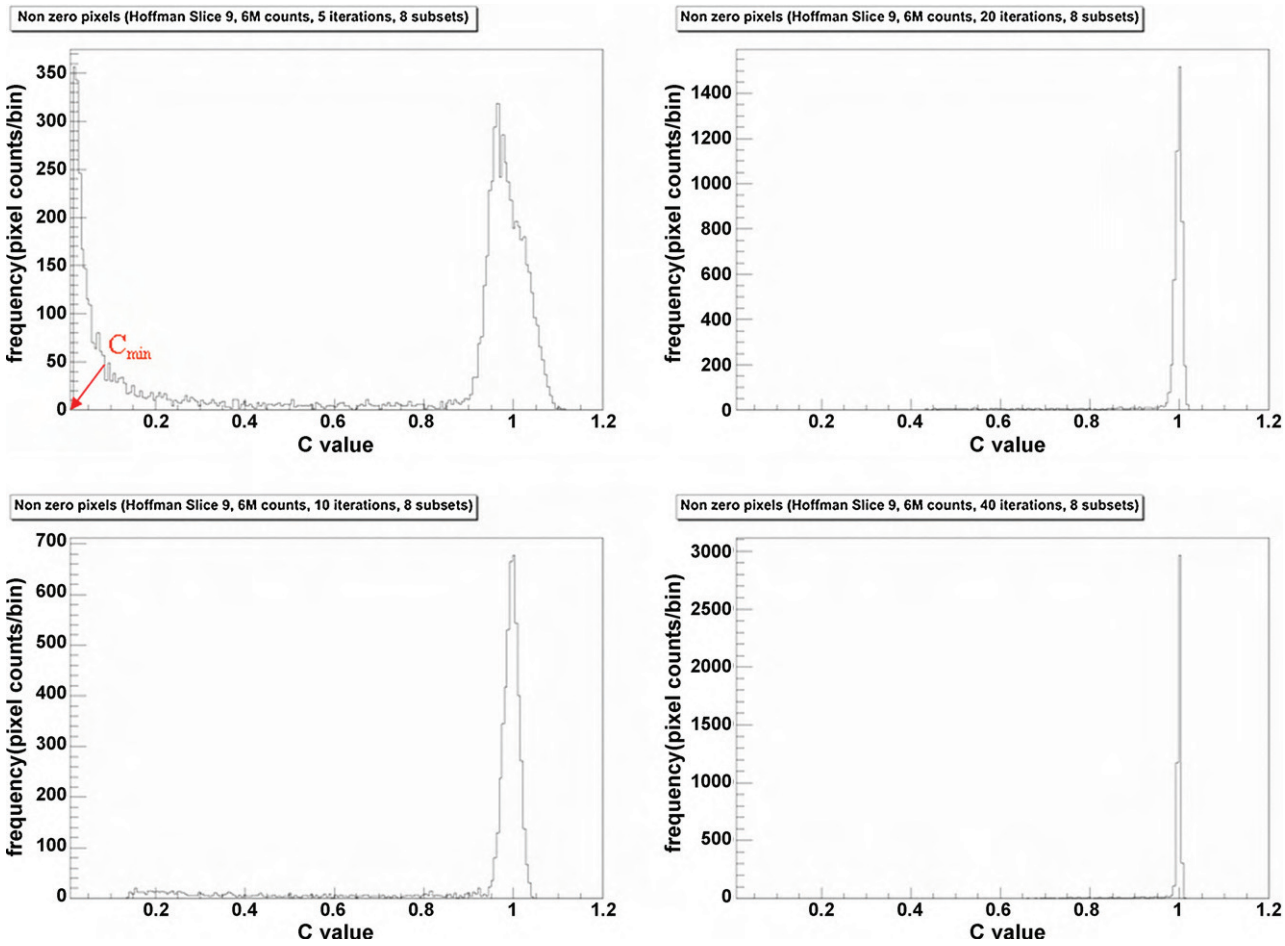

Fig. 7 – Histograms of the updating coefficients *C* for Hoffman slice 9 reconstructed with OSEM and 8 subsets.

Fig. 9b–d shows the same results for activities of 4 M, 2.1 M, and 1 M counts, respectively. All four plots show that for a given number of subsets C_{min} increases monotonically with the image activity. This is shown better in Fig. 10a–d for Hoffman slice 14, where the dependence of C_{min} versus the NRMSD is plotted for the same number of subsets in each figure having the different activities in the source as a parameter.

We have repeated the simulation for all the Hoffman brain phantom slices for activities from 0.2 to 6.0 M counts. In each case, the optimum minimum value of *C* histogram ($C_{\min}^{opt}$) was recorded following the rule:

$$C_{\min}^{opt} \equiv \left\{ C_{\min}^{(k)},\ k = \text{iteration at minimum NRMSD} \right\} \quad (5)$$

For each source activity, the value of $C_{\min}^{opt}$ was calculated and averaged over all slices. The results are plotted in Fig. 11 for 2, 4, 8, and 16 subsets along with the results from 1 subset [18], meaning MLEM. The error bars for each point illustrate the uncertainty for each measurement of $C_{\min}^{opt}$. As the number of subsets is increased, the errors are increased too, denoting that a relation between the number of subsets and the total number of line of responses (LORs) has a crucial role in the behavior of $C_{\min}^{opt}$.

8. Discussion

The results presented above (Figs. 6 and 7) show clearly that the minimum value, C_{min}, of the updating coefficients increases monotonically towards 1.0 as the number of iterations increase and that there is a clear instance where the image quality indicator, NRMSD, becomes minimum (Figs. 9 and 10), defining thus the corresponding optimum value of $C_{\min}^{opt}$ and, therefore, the iteration at which one can stop the algorithm in order to obtain the optimal image. This value, $C_{\min}^{opt}$, depends on (a) the activity of the image and (b) the number of subsets.

Fig. 11 shows that for a given number of subsets the quantity $C_{\min}^{opt}$, plotted as a function of the total activity, grows monotonically with a considerable slope at the beginning, and then with a much smaller rate for larger values of the total activity, showing a tendency to saturate. The plot shows similar behavior for all different number of subsets. The values of $C_{\min}^{opt}$ near saturation for a given total activity become smaller as the number of subsets increase. It should be noticed that for number of subsets $n_s = 1$ (MLEM), the saturation value is the largest and that the behavior for each number of subsets is described by a different curve in the plot.

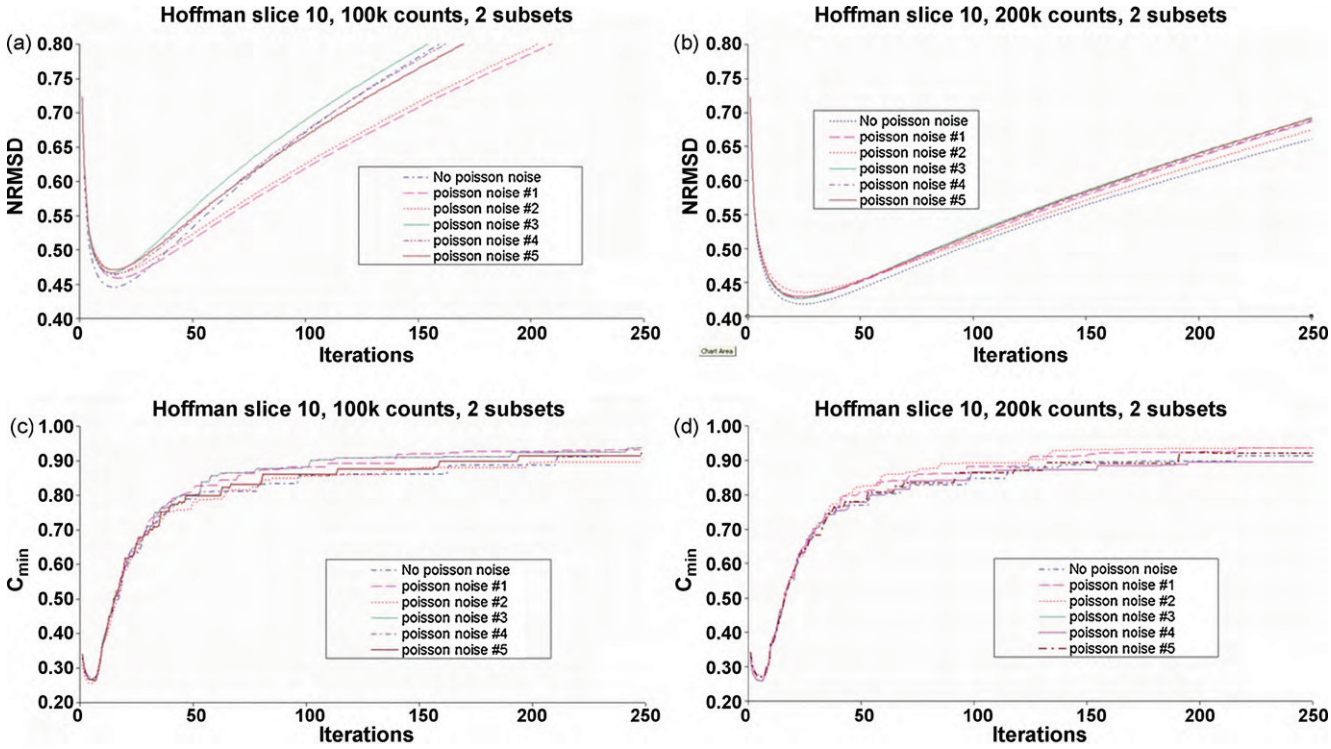

Fig. 8 – The plots of the NRMSD and C_{min} versus number of iterations, for Poisson and no Poisson noise images of Hoffman slice 10 with 100*k* and 200*k* counts.

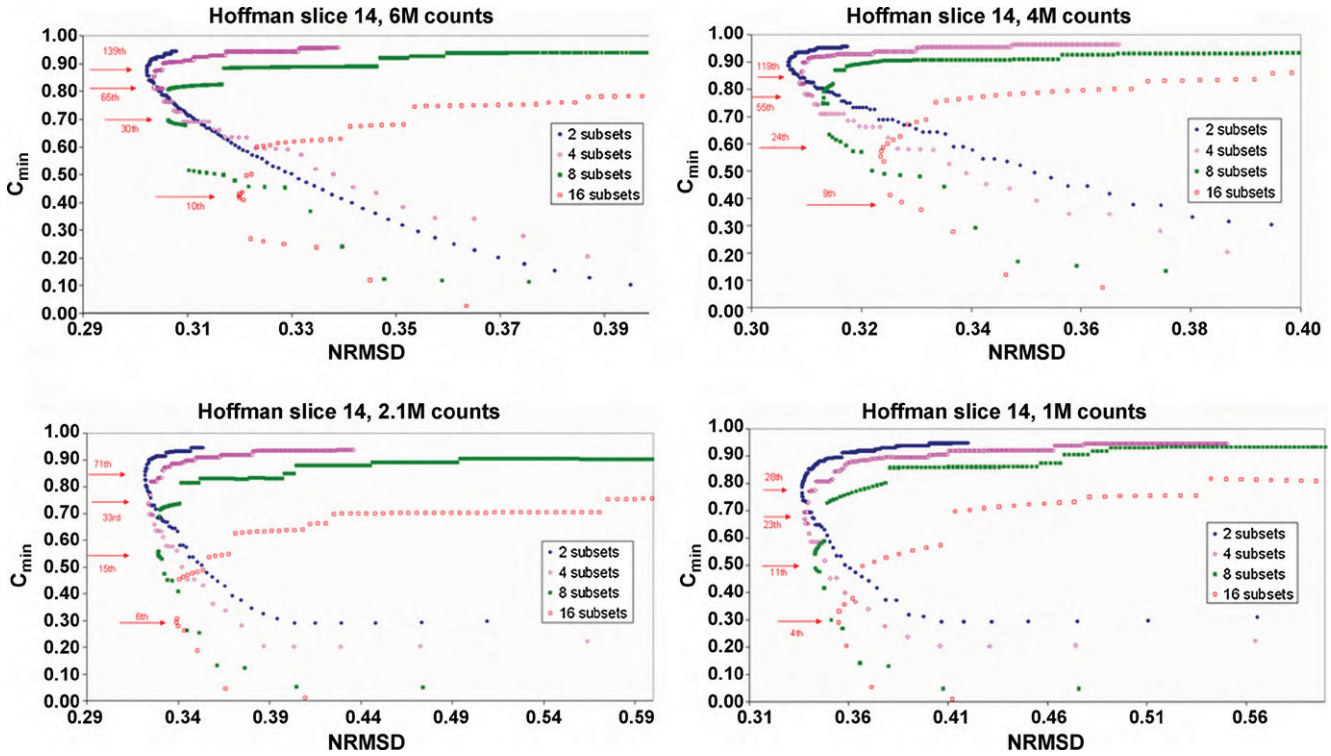

Fig. 9 – C_{min} versus NRMSD for 2, 4, 8 and 16 subsets for Hoffman brain phantom slice 14 and activity of (a) 6 M, (b) 4 M, (c) 2.1 M and (d) 1 M counts. The optimal C_{min} is where the NRMSD is minimum, and clearly the corresponding iteration number is different for different subsets (see red arrows). The behavior is similar for different activities. (For interpretation of the references to color in this figure legend, the reader is referred to the web version of the article.)

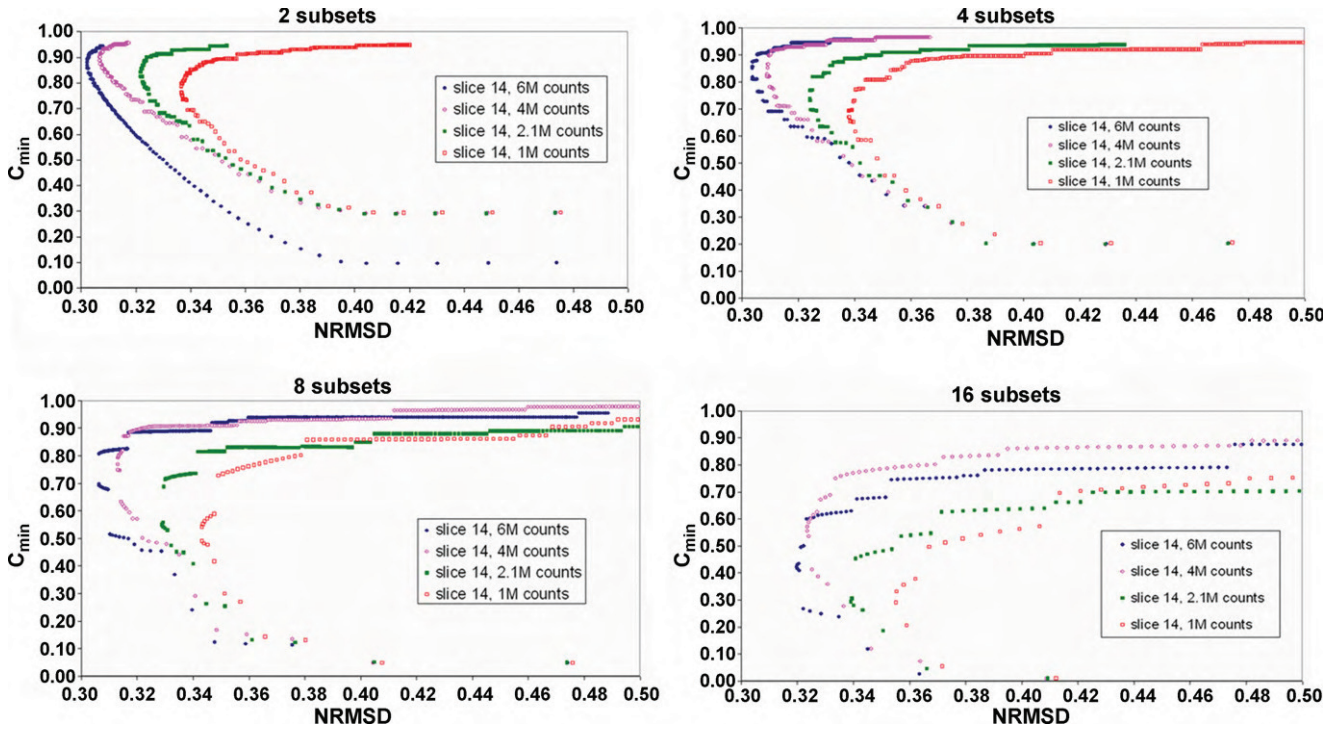

Fig. 10 – C_{min} versus NRMSD for slice 14, and different activities for all subsets. The optimal C_{min} increases with activity: (a) 2 subsets, (b) 4 subsets, (c) 8 subsets and (d) 16 subsets.

This is shown better in Fig. 12 where we plot the value of $C_{\min}^{opt}$ versus the number of subsets, using the total activity as a fixed parameter. In Fig. 12 the horizontal axis denotes the base-2 logarithm of the number of subsets (e.g. value 2 means $2^2 = 4$ subsets).

Thus, it becomes clear that the results of the study of the MLEM algorithm ($n_s = 1$) cannot predict the case of OSEM for various numbers of subsets. Figs. 11 and 12 described a unified picture of MLEM and OSEM reconstruction.

The results of our study show that for a given scan with a given number of total counts one can reconstruct the optimum image by selecting the reconstruction algorithm with a chosen number of subsets. At each iteration the value of C_{min} results from the data and can be compared with the value

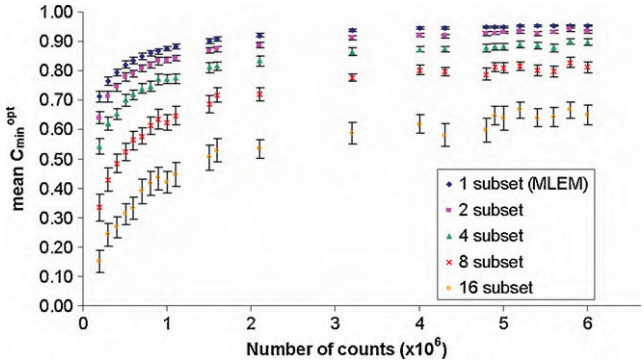

Fig. 11 – C_{min} averaged over all Hoffman phantom slices as a function of image activity for 1 (MLEM), 2, 4, 8 and 16 subsets.

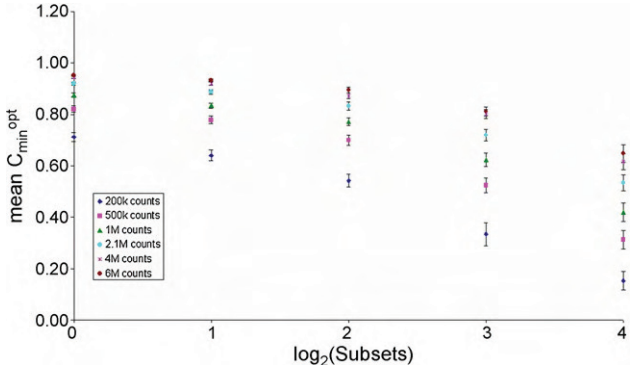

Fig. 12 – C_{min} averaged over all Hoffman phantom slices as a function of the base-2 logarithm of the number of subsets for several image activities.

of $C_{\min}^{opt}$ shown in Fig. 11 for the corresponding number of subsets.

The effect of Poisson noise was shown in the plots of Fig. 8. As shown there, the effect is not significant for large total activity and shows variations in the vicinity of minimum NRMSD of the order of 5% for activity of 100*k* counts, becoming smaller at higher total activities. The effect of Poisson statistics is shown via the error bars in Figs. 11 and 12. For $n_s = 1$ (MLEM) the total number of counts is used in the estimation of C_{min}, whereas for $n_s = 16$ only 1/16 of the data is used in each estimation of C_{min}, resulting to an uncertainty increase by a factor $\sqrt{16} = 4$, consistent with Poisson statistics.

9. Conclusions

We have studied the properties of the updating coefficients in the OSEM algorithm for image reconstruction in PET. We have employed Monte Carlo methods for the modeling of the data acquisition process for a PET tomograph and the calculation of its system matrix for iterative image reconstruction using the OSEM algorithm. The digitized Hoffman brain phantom has been employed for the generation of synthetic projection data both in a noise-free case and a case in which random Poisson noise has been added. The properties of the pixel updating coefficients, C, for the OSEM iterative image reconstruction algorithm have been analyzed and the effect of Poisson noise on the image quality has been found to be negligible. Their values for the areas in the phantom with non-zero activity have been shown to follow a distribution with a tail (values below 1.0) and a peak (values around 1.0). As the iteration process progresses, the peak of this distribution becomes narrower while the tail shifts to higher values close to 1.0. Based on these data, the relationship between C_{min} and the NRMSD has been studied as a function of total activity in the source and the number of subsets employed in the reconstruction. It should be stressed that the value of C is estimated from the data at each iteration. This study has shown that, at a given iteration, the image quality depends on the number of subsets for the PET scanner geometry simulated here. Using averaged data from all image slices of the Hoffman brain phantom a direct correlation has been found between the average values $C_{\min}^{opt}$ and the number of counts detected. Hence, the behavior of the values of the pixel updating coefficients can be correlated to a known parameter. The aim of this work is to study the behavior of the updating coefficient of OSEM algorithm and to try to define a relation between a minimum number of subsets per total number of LORs. The present work was focused in pointing at the properties of the updating coefficients in relationship to the quality of the reconstructed images using OSEM and studying the dependence on total activity and number of subsets. Our future plan is to expand this study in order to use these properties in defining a stopping rule for OSEM in a similar way that we did for MLEM [18]. We also want to study the effect of various configurations of PET scanners. In addition, we plan to study noise effects resulting from attenuation and scatter, using well validated simulation software packages, such as GATE [24]. These studies shall be the subject of a separate publication.

Conflict of interest

There is no conflict of interest for any of the five authors.

REFERENCES

[1] M.E. Juweid, B.D. Cheson, Positron-emission tomography and assessment of cancer therapy, N. Eng. J. Med. 354 (2006) 496–507.

[2] K. Herholz, W.D. Heiss, Positron emission tomography in clinical neurology, Mol. Imag. Biol. 6 (4) (2004) 239–269.

[3] K.T. Tarakji, R. Brunken, P.M. McCathy, O. Al-Checakie, A. Abdel-Latif, C.E. Pothier, et al., Myocardial viability testing and the effect of early intervention in patients with advanced left ventricular systolic dysfunction, Circulation 113 (2006) 230–237.

[4] R. Frank, R. Hargreaves, Clinical biomarkers in drug discovery and development, Nat. Rev. Drug Discov. (2) (2003) 566–580.

[5] I.K. Hong, et al., Ultra fast symmetry and SIMD-based projection-backprojection (SSP) algorithm for 3-D PET image reconstruction, IEEE Trans. Med. Imag. 6 (6) (2007) 789–803.

[6] L.A. Shepp, Y. Vardi, Maximum likelihood reconstruction for emission tomography, IEEE Trans. Med. Imag. 2 (1982) 113–121, MI-1.

[7] M. Hudson, R.S. Larkin, Accelerated image reconstruction using ordered subsets of projection data, IEEE Trans. Med. Imag. (13) (1994) 601–609.

[8] D.W. Townsend, Physical principles and technology of clinical PET imaging, Ann. Acad. Med. Singapore 2 (33) (2004) 133–145.

[9] J. Nuyts, et al., A concave prior penalizing relative differences for maximum a-posteriori reconstruction in emission tomography, IEEE Trans. Nucl. Sci. 49 (2002) 56–60.

[10] J. Qi, R.M. Leahy, S.R. Cherry, A. Chatziioannou, T.H. Fanquhar, High-resolution 3D Bayesian image reconstruction using the microPET small-animal scanner, Phys. Med. Biol. 43 (1998) 1001–1013.

[11] E. Veklerov, J. Llacer, Stopping rule for the MLE algorithm based on statistical hypothesis testing, IEEE Trans. Med. Imag. 4 (MI-6) (1987).

[12] E. Veklerov, J. Llacer, E.J. Hoffman, MLE reconstruction of a Brain phantom using a Monte Carlo transition matrix and a statistical stopping rule, IEEE Trans. Nucl. Sci. 35 (1) (1988).

[13] S. Holte, P. Schmidlin, A. Linden, G. Rosenqvist, L. Eriksson, Iterative image reconstruction for positron emission tomography, IEEE Trans. Nucl. Sci. 37 (2) (1990).

[14] N. Bissantz, B.A. Mair, A. Munk, A multi-scale stopping criterion for MLEM reconstruction in PET, Nucl. Sci. Symp Conf. Record 6 (2006) 3376–3379.

[15] G. Tzanakos, G. Kontaxakis, Statistical behaviour of the updating coefficient in the EM algorithm for PET, in: Proceeding Conference Record of the 1994 IEEE Nuclear Science Symposium and Medical Imaging Conference, vol. 3, 1994, pp. 1310–1314.

[16] G. Kontaxakis, G. Tzanakos, Stopping criterion for the iterative EM-MLE image reconstruction for PET, SPIE Proc. 2710 (1996) 133–144.

[17] A. Gaitanis, G. Kontaxakis, G. Panayiotakis, G. Spyrou, G. Tzanakos, The role of the updating coefficient of the ML-EM algorithm in PET image reconstruction, in: Proceedings of the Annual Congress of European Association of Nuclear Medicine (EANM), 2006, Book of Abstract.

[18] A. Gaitanis, G. Kontaxakis, G. Spyrou, G. Spyrou, G. Tzanakos, PET image reconstruction: a stopping rule for the MLEM algorithm based on properties of the updating coefficients, Comput. Med. Imaging Graph. (2009), doi:10.1016/j.compmedimag.2009.07.006.

[19] E.J. Hoffman, P.D. Cutler, W.M. Digby, J.C. Mazziotta, 3D phantom to simulate cerebral blood flow and metabolic images for PET, IEEE Trans. Nucl. Sci. 2 (NS-97) (1990) 616–620.

[20] http://root.cern.ch/drupal/.

[21] C.X. Wang, E.S. Wesley, G. Bilbro, P. Santago, Performance evaluation of filtered backprojection reconstruction and iterative reconstruction methods for PET images, Comput. Biol. Med. 28 (1998) 13–25.

[22] N. Rehfeld, M. Alber, The influence of noise in full Monte-Carlo ML-EM and dual matrix reconstructions in

positron emission tomography, Med. Phys. (9) (2006) 3498–3507.
[23] R. Boellaard, A. van Lingen, A. Lammertsma, Experimental and clinical evaluation of iterative reconstruction (OSEM) in dynamic PET: quantitative characteristics and effects on kinetic modeling, J. Nucl. Med. 5 (42) (2001) 808–817.
[24] S. Jan, G. Santin, et al., GATE: a simulation toolkit for PET and SPECT, Phys. Med. Biol. (49) (2004) 4543–4561.